ACS APPLIED ENERGY MATERIALS

www.acsaem.org

Article

Fused Porphyrin Thin Films as Heterogeneous Visible-Light Active Photocatalysts with Well-Defined Active Metal Sites for Hydrogen Generation

Ali M. Huerta-Flores, Giuseppe Bengasi, Kamal Baba, and Nicolas D. Boscher*

Cite This: *ACS Appl. Energy Mater.* 2020, 3, 9848−9855

Read Online

ACCESS | Metrics & More | Article Recommendations | Supporting Information

ABSTRACT: Metalloporphyrin-based photocatalysts have attracted great interest due to their high extinction coefficient in the visible range coupled to a catalytically active central metal ion surrounded by a highly conjugated heterocyclic macrocycle. In this work, fused copper(II) porphyrin-based conjugated polymer thin films are shown to be active electrocatalysts and photocatalysts for the heterogeneous hydrogen evolution reaction (HER). The fused copper(II) porphyrin thin films notably show a significant reduction of the overpotential required for HER in comparison to the reference nonfused porphyrin thin films. More importantly, in-depth high-resolution mass spectrometry reveals how the porphyrin substituents influence the catalytic performance of the films, with phenyl substituents enabling superior photocatalytic performances over mesityl substituents, providing insights for the engineering of heterogeneous catalysts based on fused metalloporphyrins.

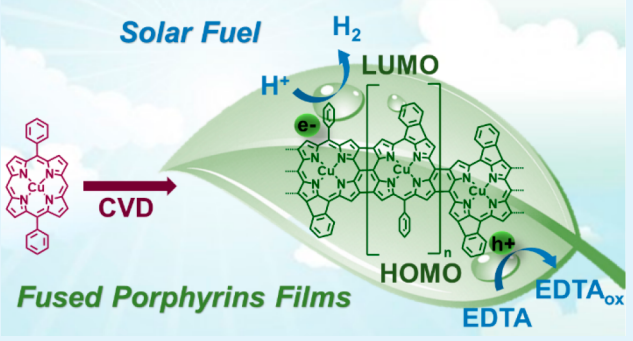

KEYWORDS: *Fused Porphyrins, Chemical Vapor Deposition, Hydrogen Evolution Reaction, Heterogeneous Catalysis, Photocatalysis*

INTRODUCTION

Metalloporphyrins and related compounds, selected by nature to fulfill the main catalytic phenomena allowing life (photosynthesis by chlorophylls and respiration by cytochromes), have been integrated into many technological applications.[1−11] In particular, the central metal ion of metalloporphyrins, surrounded by a highly conjugated heterocyclic macrocycle, can readily interconvert between different oxidation states to accomplish oxidation and reduction reactions,[1−11] including the hydrogen evolution reaction (HER),[2,3,9−11] oxygen evolution reaction (OER),[4] and oxygen reduction reaction (ORR).[5,6] In electrocatalysis, metalloporphyrins can reduce the substantial overpotential required for the HER[2,9,10] and OER reactions.[4] Owing to their strong light absorption in the visible region and their photophysical properties, metalloporphyrinoids can even further reduce (i.e., photoelectrocatalytic water splitting)[7] or suppress (i.e., photocatalysis) the need for the applied bias voltage.[8,9]

Numerous strategies have been developed to enhance the catalytic properties of porphyrins.[1−11] In particular, various central metal cations (e.g., Mn^{III},[6] Fe^{III},[6,8] Co^{II},[4,5,9] Ni^{II},[11] Cu^{II},[2] Zn^{II},[7] and Ga^{III}[10]), which can act as the hydride-binding site in HER,[10,11] have been studied. The significance of the porphyrin ligands, which can act as the electron transfer site,[10] porphyrin substituents, which can act as proton relays (e.g., carboxylic acid and amino groups), and cocatalysts[9] has also been demonstrated. The covalent grafting of porphyrins provides another strategy to further enhance their catalytic performances, as well as their stability and applicability.[7] Particularly, Xie et al. have recently attached cobalt(II) porphyrins to water-soluble polymers conveniently functionalized with carboxylic acid side-chain groups that can function as proton relays.[9] In parallel to the growing attention placed on conjugated polymer photocatalysts,[12,13] dominated by metal-free graphitic carbon nitride ($g\text{-}C_3N_4$),[14] several studies have highlighted the cooperative effect promoted by conjugated covalent links between porphyrins.[2,4,5] In addition to a stability increase, covalent cobalt(II) porphyrin frameworks exhibit improved catalytic performances for both OER,[4] with a reduced overpotential compared to a cobalt porphyrin monomer, and ORR.[5] The superior catalytic activity of the cobalt porphyrin polymer was associated with its ability to store multiple charges in order to fulfill a four-electron catalytic process, in contrast to the two-electron catalytic process usually observed for monomeric cobalt porphyrins.[15]

Received: July 1, 2020
Accepted: October 2, 2020
Published: October 14, 2020

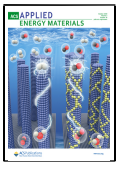

https://dx.doi.org/10.1021/acsaem.0c01545
ACS Appl. Energy Mater. 2020, 3, 9848−9855

Very recently, directly fused copper(II) porphyrin dimers have shown to be highly active homogeneous catalysts for HER.[2] Once again, the conjugated linkage of fused porphyrin dimers allow us to significantly improve the electrocatalytic performances and reduce the required overpotential in comparison to the respective nonfused monomeric porphyrin.[2] Nevertheless, these promising observations on fused copper(II) porphyrin dimers[2] are overshadowed by the difficulties related to the synthesis of longer directly fused porphyrin oligomers and their integration as heterogeneous catalysts.[16] In a general manner, in spite of their attractive electronic,[16,17] electrochemical[2] and optical properties,[16,17] including an extremely red-shifted absorption up to the infrared region when multiply fused,[17] directly fused porphyrins struggle to meet the requirements of practical applications due to their very weak solubility and nonmeltability.[16] Gas phase methods toward the synthesis of fused porphyrins directly on a surface have recently been developed to circumvent the limitation related to solution-based approaches.[18,19] Notably, the sublimation under ultrahigh vacuum of porphyrins onto oriented metal surfaces, e.g., Cu(110)[18] or graphene,[19] has been reported to yield the formation of fused porphyrin submonolayers. More recently, the gas phase reaction of metalloporphyrins with suitable oxidants has provided a simple, reliable, and scalable gas phase route toward the simultaneous synthesis and deposition of fused porphyrin thin films onto virtually any substrate.[20−22] Beyond overcoming many of the limitations to the practical use of fused porphyrin tapes,[20] the chemical vapor deposition (CVD) reaction of metalloporphyrins enables the synthesis of fused porphyrins chelating different metal cations, including copper(II),[21] or bearing substituents other than the bulky solubilizing ones used in solution-based approaches.[22]

On the basis of this recent development, we investigate in this report the heterogenization of directly fused metalloporphyrins for catalysis. Heterogenization is desirable to prevent deactivation due to photobleaching or solvolysis and easy recovery from the reaction media.[1] Beyond, we take advantage for the first time of the exceptional light absorbance of directly fused porphyrins for photocatalysis. In particular, we report the visible-light-driven hydrogen evolution reaction using directly fused metalloporphyrin thin films and using ethylenediaminetetraacetic acid (EDTA) as the sacrificial agent. The synthesis of the directly fused metalloporphyrin thin films is evidenced by ultraviolet−visible−near-infrared (UV/vis/NIR) analysis, laser desorption ionization high-resolution mass spectrometry (LDI-HRMS), and X-ray photoelectron spectroscopy (XPS), while their characterization is completed by (photo)electrical and (photo)electrochemical investigations that reveal the significance of both the intermolecular and intramolecular dehydrogenative coupling of the porphyrins.

RESULTS AND DISCUSSION

Preparation and Characterization of the Fused Copper(II) Porphyrin Thin Films. The fused porphyrin thin films (**pCuDMP** and **pCuDPP**) were prepared via oxidative chemical vapor deposition (oCVD)[23] (Scheme S1 and Table S1 for details on the oCVD reaction conditions). With the aim to form large fused porphyrin tapes that can store and delocalize multiple charges, disubstituted porphyrin motifs were selected.[24] Following the recent report by Khusnutdinova et al. on the superior electrocatalytic properties of binuclear copper(II) fused porphyrins for HER,[2] copper(II) and mesityl groups were chosen as the central metal ion and *meso*-susbtituents, respectively (Chart 1a). In addition to copper(II) 5,15-(dimesityl)porphyrin (CuDMP), copper(II) 5,15-(diphenyl)porphyrin (CuDPP) (Chart 1c) was investigated due to the enhanced $\pi-\pi$ interactions and improved electrical conductivity when using phenyl groups as substituents.[21] Iron(III) chloride ($FeCl_3$) was selected as the oxidant owing to its ability to promote the synthesis of directly fused porphyrins in oCVD.[25] To ensure a sufficient dehydrogenative coupling efficiency, $FeCl_3$ was sublimed in excess with respect to the porphyrin monomers (Table S1).

Chart 1. Molecular Structures of (a) Copper(II) 5,15-(Dimesityl)porphyrin (CuDMP) and (c) Copper(II) 5,15-(Diphenyl)porphyrin (CuDPP), Whose Intermolecular Dehydrogenative Coupling Reaction under Vacuum Condition Yields the Formation of Doubly and Triply Fused (b) pCuDMP and (d) pCuDPP Tapes, Respectively[a]

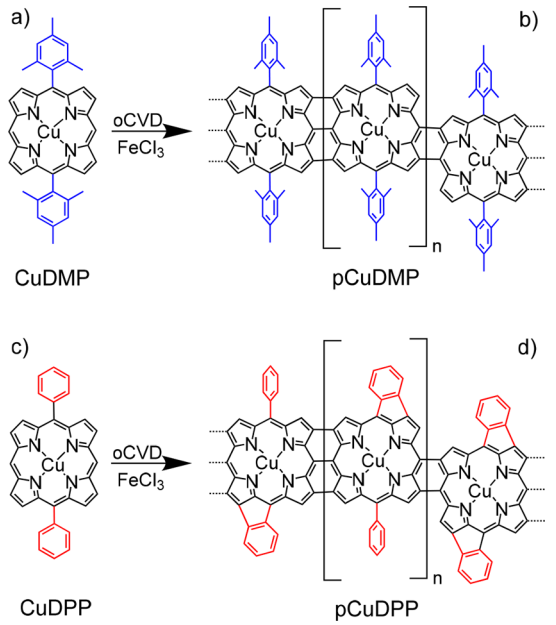

[a]For CuDPP, which possesses free *ortho* positions on the phenyl ring, intramolecular dehydrogenative coupling occurs between the phenyl substituent and the porphyrin macrocycle.

Naked-eye observation and UV/vis/NIR spectroscopy of the **pCuDMP** and **pCuDPP** thin films deposited on glass reveals the characteristic extension of the absorption to longer wavelengths (Figure 1), confirming the formation of fused porphyrin tapes.[16,17] The oxidative polymerization reaction is readily detectable from the dark gray (**pCuDMP**) to dark green (**pCuDPP**) colorations of the oCVD thin films that contrast with the vivid orange color of the reference **sCuDMP** and **sCuDPP** thin films prepared by sublimation of CuDMP and CuDPP without $FeCl_3$, respectively (Figure 1, insets). More importantly, the extension of the absorption spectra to the NIR for both **pCuDMP** (Figure 1a) and **pCuDPP** (Figure 1b) indicates the formation of multiply fused porphyrin tapes (Chart 1b and d).[16,17,25] One should highlight the splitting of the Soret band for the **sCuDPP** thin film that indicates $\pi-\pi$ stacking interactions between the CuDPP molecules.[26] This enlargement of the Soret band is not observed for **sCuDMP** since the mesityl groups, more prone to arrange orthogonally

https://dx.doi.org/10.1021/acsaem.0c01545
ACS Appl. Energy Mater. 2020, 3, 9848−9855

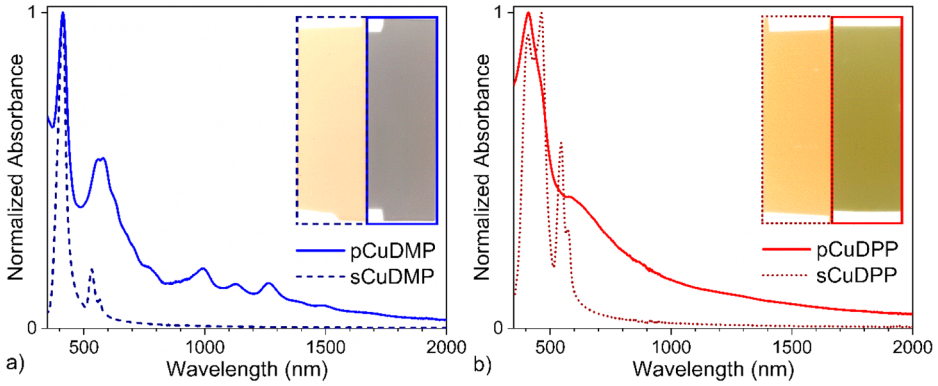

Figure 1. UV/vis/NIR absorption spectra and optical images of the (a) **pCuDMP** (blue) and (b) **pCuDPP** (red) thin films deposited on glass substrates. The UV/vis/NIR absorption spectra and optical images of the **sCuDMP** and **sCuDPP** reference thin films obtained from the sublimation of CuDMP and CuDPP, respectively, are provided for comparison.

to the porphyrin macrocycle,[27] increase the intermolecular distance and weaken the $\pi-\pi$ interactions.

LDI-HRMS confirms the successful synthesis of fused copper(II) 5,15-(dimesityl)porphyrin oligomers (Figure S1a,b) in agreement with a previous report.[21] LDI-HRMS also confirms the formation of fused copper(II) 5,15-(diphenyl)porphyrin oligomers from the gas phase reaction of CuDPP and $FeCl_3$ (Figure S1c,d), which is not surprising since nickel(II) porphyrins substituted with phenyl groups are known to readily form fused porphyrin tapes in oCVD.[20,24] Alongside the targeted intermolecular dehydrogenative coupling reaction, exchange of hydrogen atoms by chlorine, leading to several sets of peak clusters separated by 35 mass units, is detected in the mass spectra of both **pCuDMP** and **pCuDPP** (Figure S1). Chlorination, already observed during the oCVD of metalloporphyrins,[22,24,25] is confirmed by XPS that reveals the presence of two chlorine environments associated with the metal chloride environment related to the presence of unreacted $FeCl_3$ or $FeCl_2$ byproducts in both **pCuDMP** and **pCuDPP** and to organic chloride related to the chlorination of the porphyrins (Figure S2). Chlorination of the porphyrins originates from a reaction between the porphyrin and $FeCl_3$ or Cl_2 produced from $FeCl_3$ during the sublimation step.[28] Mass spectrometry or XPS did not allow the identification of any preferential reactive site on the porphyrin for chlorination, and chlorine can occupy both the porphyrin core and the phenyl or mesityl ring. Chlorination is known to decrease the solubility of porphyrin systems,[29] which could be an asset for heterogeneous catalysis as it stabilizes the fused porphyrin thin films.

Enlargement of the dimer regions of the LDI-HRMS spectra of the **pCuDMP** and **pCuDPP** thin films (Figure 2) confirms the formation of multiple C−C bonds between the porphyrin units. The LDI-HRMS spectra of the **pCuDMP** are notably dominated by peaks related to the formation of doubly and triply fused CuDMP dimers, $[(CuDMP)_2-H_4]^+$ and $[(CuDMP)_2-H_6]^+$. While the maximum number of 2H pairs eliminated for the CuDMP dimer is limited to three (Figure 2a), **pCuDPP** exhibits up to the loss of six 2H pairs for the CuDPP dimer (Figure 2b). The elimination of 12 hydrogen atoms is rendered possible by the free *ortho* positions on the phenyl rings that allow intramolecular dehydrogenative coupling between the phenyl substituent and the porphyrin core.[22] Intramolecular dehydrogenative coupling, occurring simultaneously to the intermolecular dehydrogenative coupling

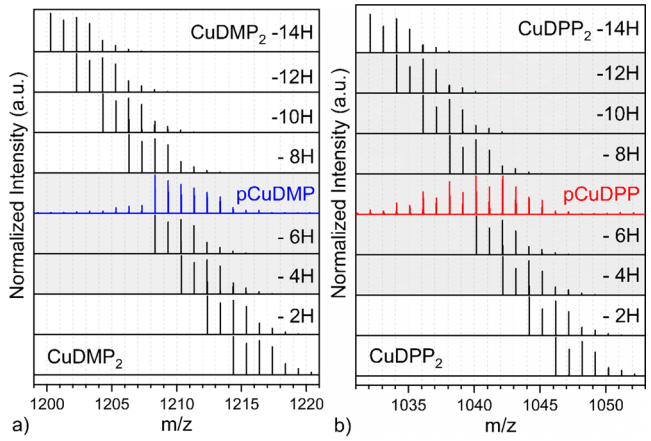

Figure 2. LDI-HRMS spectra of the (a) $(CuDMP)_2$ (blue) and (b) $(CuDPP)_2$ (red) regions for the **pCuDMP** and **pCuDPP** thin films. The simulated patterns of $[(CuDMP)_2-(H_2)_n]^+$ and $[(CuDPP)_2-(H_2)_n]^+$ (n comprised between 0 and 7) (dark) are provided for the ease of comparison.

reaction, can theoretically yield up to the loss of seven 2H pairs for $\beta-\beta$/*meso-meso*/$\beta-\beta$ triply linked CuDPP dimers in which the four phenyl rings are fused to the porphyrin cores.[24] This cyclization between the phenyl rings and porphyrin macrocycle is known to induce flattening of fused porphyrin tapes, enhancing $\pi-\pi$ interactions, and finally improving the electrical conductivity of the fused porphyrin thin films.[22]

In both **pCuDMP** and **pCuDPP**, no signal related to the presence of the free-base porphyrin (H_2DPP) monomer or oligomers is detected, confirming that the copper(II) ion is effectively retained in the porphyrin core during oCVD reaction. In addition, aside from the small incorporation of iron (ca. 2.0 at. %) and chlorine (2.7 at. %) originating from the oxidant, the relative atomic compositions obtained by XPS of the **pCuDMP** and **pCuDPP** thin films are close to the one of their reference counterpart (**sCuDMP** and **sCuDPP**) and to the theoretical ones of their respective monomers (Table S2). More importantly, the binding energies of the Cu $2p_{3/2}$ core level of **pCuDMP** and **pCuDPP** at 934.6 and 934.4 eV are indicative of a copper(II) oxidation state (Figure S3). These contributions are associated with a characteristic broad shakeup satellite spreading between 941 and 945 eV. No contribution related to the copper(I) oxidation state is observed at lower binding energy (ca. 933 eV),[30] confirming

https://dx.doi.org/10.1021/acsaem.0c01545
ACS Appl. Energy Mater. 2020, 3, 9848−9855

that no degradation or demetalation of the metalloporphyrins occur during the oCVD process.

Electrical and Electrochemical Characterization of the Fused Porphyrin Thin Films. Importantly, in the perspective to use fused metalloporphyrin tapes as heterogeneous catalysts, scanning electron microscopy confirms that all the thin films cover the whole surface substrate and are pinhole free (Figures S7 and S8). The conductivity measurements of the fused porphyrin and reference thin films deposited onto commercial OFET chips evidence a 5 orders of magnitude increase of the conductivity when ensuring the intermolecular dehydrogenative coupling of the porphyrin units (Figure S9). Specifically, the conductivity rises from 10^{-11} S cm^{-1} to 10^{-6} S cm^{-1} and from 10^{-8} S cm^{-1} to 10^{-3} S cm^{-1} when fusing CuDMP and CuDPP, respectively. One should note that in accordance to our prior report,[22] the phenyl substituents grant a several order of magnitude higher conductivity in comparison to the mesityl groups. Electrochemical impedance spectroscopy (EIS) analysis under both dark (Figure 3) and light

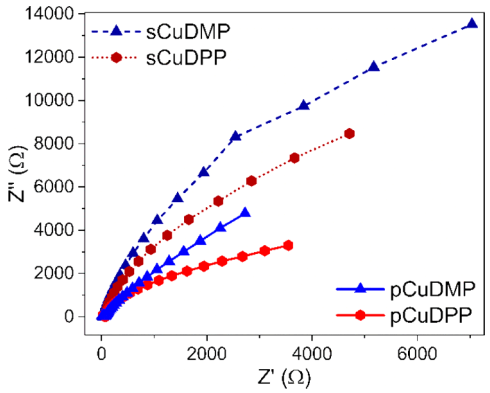

Figure 3. Nyquist plots of the fused porphyrin (**pCuDMP** and **pCuDPP**) and reference (**sCuDMP** and **sCuDPP**) thin films measured in the dark at E = 0.4 V_{RHE}.

conditions (Figure S10) confirms the lower resistance of the fused porphyrin thin films (**pCuDPP** and **pCuDMP**) over their reference counterparts (**sCuDPP** and **sCuDMP**). This is related to the formation of multiply fused porphyrin chains,[25] such as evidenced by UV/vis/NIR (Figure 1) and LDI-HRMS (Figure S1). Beyond this, the Nyquist plot measured for **pCuDPP** exhibits a shorter radius of the semicircle compared to the one of **pCuDMP**, indicating a faster charge transference, lower resistance, and reduced recombination of charges for **pCuDPP**. Such behavior arises from (i) the smaller size of the phenyl substituent and (ii) its ability to promote intramolecular dehydrogenative cyclization with the porphyrin core, such as evidenced by HRMS (Figure 2). Indeed, a smaller substituent size and flattening of the molecules, induced by a cyclization between the free *ortho* position of aryl groups and the porphyrin core, are both known to drastically enhance the electronic properties of the films due to increased $\pi-\pi$ interactions.[22]

Mott−Schottky measurements were carried out to determine the flat band potential and the charge carrier density in the thin films (Figure 4). Surprisingly, all the samples exhibit a positive slope, indicating an n-type conductivity. This could be rationalized considering two aspects, i.e., where (i) the water-based electrolyte used for the measurement may act as an electron donor toward the porphyrin-based thin films causing a

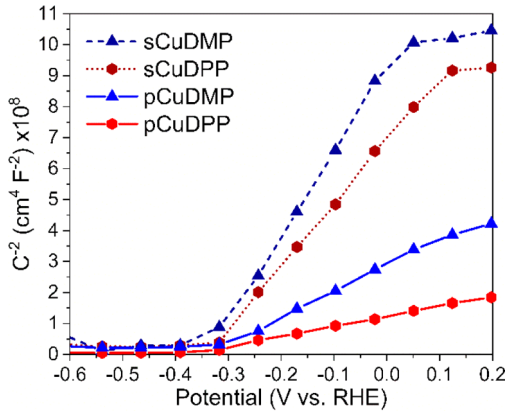

Figure 4. Mott−Schottky plots of the fused porphyrin (**pCuDMP** and **pCuDPP**) and reference (**sCuDMP** and **sCuDPP**) thin films.

dedoping of the polymers and (ii) the supramolecular assembly of the fused porphyrin tapes influences the charge carrier species. Indeed, Aida et al. observed that changing the π-stacking of fused copper(II) porphyrin dimers possibly switches their preference for carrier species,[31] with the ones expected for the fused porphyrin thin films[22] behaving as n-type conductors. In this type of semiconductor, the flat band potential (V_{fb}), determined from the intercept of the linear fitting with the x-axis, corresponds to the bottom of the conduction band (CBM). The fused porphyrin and reference thin films exhibit almost identical values of flat band potential, ca. −0.3 V_{RHE} (Table 1 and Figure S11). The donor density

Table 1. Donor Density (N_D), Flat Band Potential (V_{fb}) and Valence Band Maximum (VBM) for the Fused Porphyrin (pCuDMP and pCuDPP) and Reference (sCuDMP and sCuDPP) Thin Films

	conductivity	N_D (cm^{-3})	V_{fb} (V_{NHE})	VBM (V_{NHE})
sCuDMP	n-type	6×10^{18}	−0.33	1.90
pCuDMP		20×10^{18}	−0.31	0.63
sCuDPP		7×10^{18}	−0.35	2.30
pCuDPP		50×10^{18}	−0.34	1.20

(N_D) values (Table 1), estimated from the slope of the linear fitting, indicate a stronger influence of the intermolecular dehydrogenative coupling reaction on the concentration of charge carriers than the intramolecular dehydrogenative coupling reaction. In particular, while the donor density is increased from 1 order of magnitude upon oxidative polymerization of the porphyrins, it is only doubled when selecting the phenyl group over mesityl. Thus, **pCuDPP** exhibits the lowest slope (Figure 4) and the highest charge carrier concentration (50×10^{18} cm^{-1}), which relates with the highest conductivity of **pCuDPP** (Figure 3) and should favor the separation and transport of charges.[32]

Photoemission measurements (XPS) were performed to further study the electronic structure of the films (Figure 5a). In each case, the dehydrogenative coupling of the porphyrins produced a shift in the valence band (VB) edge toward lower binding energies (Table S3). In particular, the valence band maxima (VBM), determined from the extrapolation of the linear fit of the leading edges of the spectra to the baseline, of the CuDMP and CuDPP-based thin films are shifted from 1.90 to 0.63 V_{NHE} and 2.30 to 1.20 V_{NHE}, respectively (Table 1).

https://dx.doi.org/10.1021/acsaem.0c01545
ACS Appl. Energy Mater. 2020, 3, 9848−9855

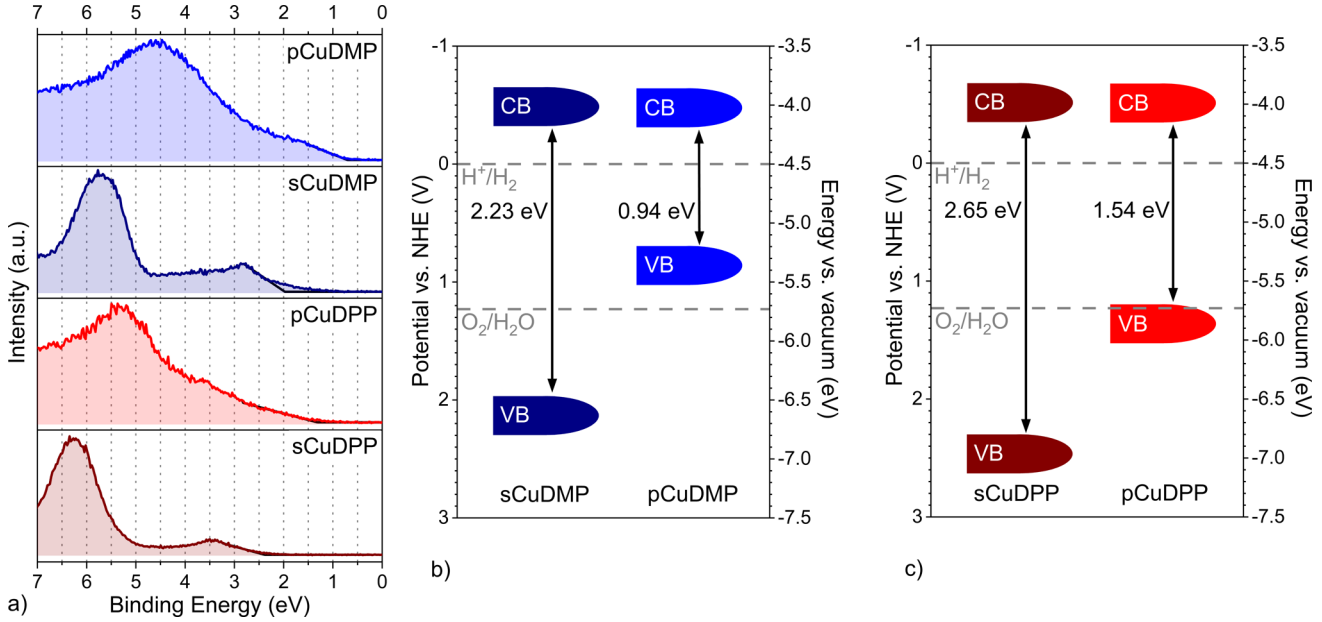

Figure 5. (a) Valence band (VB) edge XPS spectra for the fused porphyrin (**pCuDMP** and **pCuDPP**) and reference (**sCuDMP** and **sCuDPP**) thin films. The black lines show the linear extrapolation of the leading edges of the spectra to the baseline used to extract the valence band maximum (VBM). (b, c) Schematic illustration of the band structures and potentials of the fused porphyrin and reference thin films prepared from (b) CuDMP and (c) CuDPP.

This observation is consistent with the expansion of π-electronic system known to raise the energy of the highest occupied molecular orbital (HOMO).[17] Given the almost constant position of the CBM, shifting of the VBM to lower binding energies (BE) results in a reduced band gap for the fused porphyrin thin films (Figures 5). The lower band gap of **pCuDMP** (0.94 eV) compared to **pCuDPP** (1.54 eV) suggests the formation of longer fused porphyrin tapes when using mesityl substituents (Table S4). The mesityl groups are assumed to enable a greater mobility of the porphyrin units, contributing to an increase of the number of porphyrins forming the tapes, by preventing their $\pi-\pi$ stacking. In addition, the intramolecular cyclization occurring when using phenyl substituents may compete with the intermolecular coupling in the **pCuDPP** thin film.

Electrocatalytic Activity for HER. Based on the recent report on the superior performances of fused copper(II) porphyrin dimer over nonfused copper(II) porphyrin as a homogeneous molecular electrocatalyst for HER,[2] the extended fused copper(II) porphyrin tapes reported in this work are investigated as heterogeneous electrocatalysts. In order to enable a fair comparison of the fused porphyrin and reference thin film performances, similar catalyst loadings (ca. 30 μg cm^{-2}) were investigated for each of the investigated deposition conditions (Table S2). The HER polarization curves were obtained through linear sweep voltammetry (LSV) under dark conditions for the porphyrin-based thin films deposited on FTO substrates (Figure 6). While **sCuDMP** and **sCuDPP** exhibit poor currents in the range of potential studied, the fused porphyrin thin films (**pCuDMP** and **pCuDPP**) show significant cathodic current (several mA cm^2) from -0.4 V_{RHE} and -0.2 V_{RHE}, respectively. The overpotential required for HER for the fused porphyrin thin films is competitive compared to the overpotential reported for several noble-metal free electrocatalysts.[33,34] For example, MoS_2 requires an overpotential of -0.16 V_{RHE} for performing

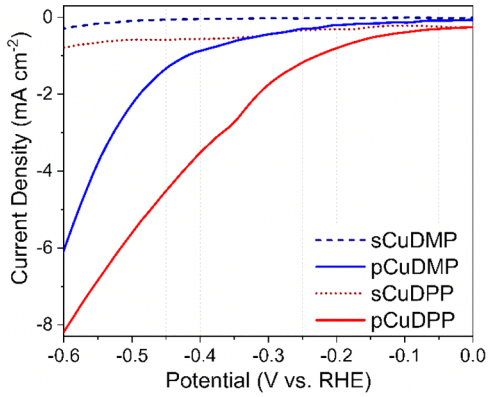

Figure 6. Electrocatalytic performance for HER of the fused porphyrin (**pCuDMP** and **pCuDPP**) and reference (**sCuDMP** and **sCuDPP**) thin films.

HER.[35] Though the currents generated may appear moderate, they are consistent with the low catalyst loading, ca. 30 μg cm^{-2} in the present work, while several mg cm^{-2} are typically investigated.[34] As a comparison point, low weight per unit area (8.5 μg cm^{-2}) vertically aligned MoS_2 films exhibit a current density of 8 mA cm^2 at an overpotential of -0.4 V_{RHE}.[36] These results highlight the suitability of fused porphyrin thin films to serve as heterogeneous electrocatalysts. The lower overpotential observed in the fused porphyrins (**pCuDMP** and **pCuDPP**) in comparison to the nonfused porphyrins (**sCuDMP** and **sCuDPP**) is directly related with the extension of the π-electron conjugation known to enable the efficient separation and storage of multiple charges.[2,4,5,15,37] Interestingly, the electrocatalytic performances of the fused porphyrin thin films are highly stable over multiple cycles (Figure S12a), demonstrating their suitability for electrocatalytic applications.

Photocurrent Response and Photocatalytic Activity for HER. Porphyrins are strong chromophores that can be employed for light energy harvesting and charge transfer in

https://dx.doi.org/10.1021/acsaem.0c01545
ACS Appl. Energy Mater. 2020, 3, 9848−9855

photoinduced processes.[1,3,8,38] Both the reference and fused porphyrin thin films deposited on FTO substrate exhibit a lower charge transfer resistance under light irradiation, such as expressed by the smaller impedance arc radius (Figure S10). The photocurrent response of the fused porphyrin thin films was studied through transient photocurrent measurements performed at equilibrium potential (Figure 7). One should

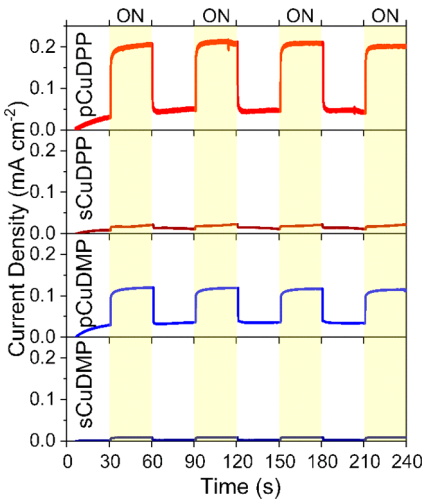

Figure 7. Transient photocurrent measurements under visible light irradiation (450 W) for the fused porphyrin (**pCuDMP** and **pCuDPP**) and reference (**sCuDMP** and **sCuDPP**) thin films.

note here that irradiation of the pristine FTO substrate did not yield photocurrent generation (Figure S17). The porphyrin-based thin films exhibit a positive photocurrent upon irradiation, characteristic of n-type semiconductors, which confirms that the samples have electrons as majority carriers. The fused porphyrins (**pCuDMP** and **pCuDPP**) exhibited a far higher photocurrent response than their reference counterpart (**sCuDMP** and **sCuDPP**). This behavior is attributed to a superior light absorption, such as illustrated by the UV/vis/NIR measurements, and a more effective charge generation and separation in the fused porphyrin thin films. Indeed, the intermolecular dehydrogenative coupling between the porphyrin units ensures the extension of the π-electron conjugation in **pCuDPP** and **pCuDMP**, which directly relates to a lower recombination of charges. On the other hand, the absence of a covalent conjugated bond between the porphyrins in the reference thin films (**sCuDMP** and **sCuDPP**), expressed by a lower conductivity, does not prevent the recombination of charges and yields lower photocurrent responses. One should note that **sCuDPP** exhibits a higher photocurrent response than **sCuDMP**, most probably due to the favored $\pi-\pi$ stacking interactions between the porphyrin molecules in this sample. Similarly, **pCuDPP** exhibits an almost two times higher photocurrent response than **pCuDMP**, which is attributed to the smaller size of the phenyl substituents, that favored $\pi-\pi$ stacking interactions; this is also attributed to the free *ortho* positions of these phenyl substituents that enable an intramolecular dehydrogenative coupling, inducing both an increased π-electron conjugation in this sample and a further favored $\pi-\pi$ stacking interaction between the fused porphyrin tapes. Interestingly, the stability of the photocurrent response of the porphyrin-based thin films was demonstrated after several cycles of illumination, demonstrating the suitability for photo(electro)catalytic applications.

The potential of the fused porphyrin thin films for visible light photocatalysis was investigated from the hydrogen evolution reaction from water splitting using EDTA (10% in an aqueous solution, pH = 8) as a sacrificial agent. The porphyrin-based thin films, deposited on FTO substrates, were illuminated by a solar simulator integrated with a Xe lamp of 450 W (Figure S13). It is worth noting here that no photocatalytic hydrogen production was detected for the pristine FTO substrate (Figure S18). As it can be observed from the hydrogen evolution curves, the porphyrin-based thin films exhibit linear hydrogen production rates during 3 h (Figure 8a) and multiple cycles of illumination (Figure S12b), illustrating the high stability of porphyrinic compounds. Among the characterized samples, **pCuDPP** exhibits the highest hydrogen evolution rate, i.e., 9.2 μmol cm^{-2} h^{-1}. This value is over 6 times higher than the performances achieved by the **pCuDMP** thin film and the reference thin films (Figure 8b). The photocatalytic activity of the reference thin films, notably **sCuDPP**, originates from the $\pi-\pi$ stacking of the porphyrins in this films, which enable the long-standing charge separation upon visible-light illumination.[39] The superior hydrogen evolution rate of **pCuDPP** is attributed to the higher photogeneration of charge carriers (Figure 7) due to the broadening of the absorption to the whole range of the visible range (Figure 1b) and the lower charge transfer resistance (Figure 3) associated with a reduced electron–hole

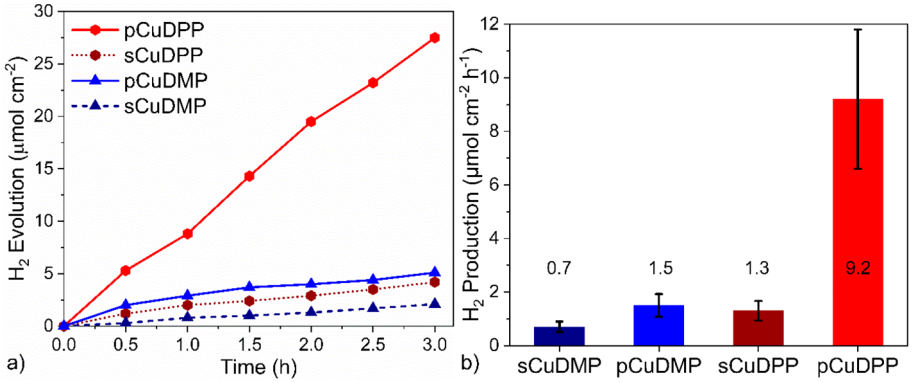

Figure 8. (a) Photocatalytic evolution of hydrogen from water by the fused porphyrin (**pCuDMP** and **pCuDPP**) and reference (**sCuDMP** and **sCuDPP**) thin films under visible-light irradiation (Xe lamp, 450 W), using EDTA (10%) as the sacrificial agent. (b) Summary of the hydrogen evolution rates in μmol cm^{-2} h^{-1}.

https://dx.doi.org/10.1021/acsaem.0c01545
ACS Appl. Energy Mater. 2020, 3, 9848–9855

recombination in the fused porphyrin thin films.[40] Therefore, the extended π-electron conjugation and superior $\pi-\pi$ stacking in **pCuDPP**, which promote a higher delocalization of the charge carriers and reduce their recombination, likely contribute to the superior photocatalytic performances of **pCuDPP** over **pCuDMP** and yield hydrogen production rates under visible light competitive with the reported ones from other porphyrin-based assemblies.[41,42]

CONCLUSIONS

In summary, fused porphyrin tapes have been successfully implemented as heterogeneous catalysts for the hydrogen evolution reaction. The intermolecular dehydrogenative coupling of di-*meso*-substituted copper(II) porphyrins enables an efficient separation and transfer of the charge carriers, considerably reducing the overpotential required for performing HER, i.e., −0.4 V_{RHE}. The intramolecular dehydrogenative coupling reaction between the free *ortho* position of the phenyl substituent and the β position of the porphyrin macrocycle, extending beyond the π-electron conjugation of the fused porphyrin tapes, enable a further decrease of the overpotential required for HER, i.e., −0.2 V_{RHE}. Dehydrogenative coupling is also responsible for a significant reduction of the band gap. Interestingly, the band gap of **pCuDPP** tightly straddles the oxidation and reduction potentials of water and provides to this sample superior a higher visible-light photocatalytic hydrogen production rate, i.e., 9.2 μmol cm^{-2} h^{-1}. Overall, the chemical vapor deposition reaction of metalloporphyrins provides a versatile and up-scalable approach toward the simultaneous synthesis and engineering of platinum group metal-free heterogeneous catalysts for solar fuel production. This synthesis strategy described in this work is not specific to hydrogen production and can be implemented with other di-*meso*-substituted metalloporphyrins to mimick important biological processes or to address essential chemical reactions.

ASSOCIATED CONTENT

Supporting Information

The Supporting Information is available free of charge at https://pubs.acs.org/doi/10.1021/acsaem.0c01545.

Experimental details on the materials, CVD procedures, physical and chemical characterizations and evaluation of the catalytic performances; schematic of the CVD reactor; LDI-HRMS spectra of the thin films; relative atomic concentrations of the thin films; XPS spectra of the Cu $2p_{3/2}$, C 1s, N 1s, Cl 2p, and Fe $2p_{3/2}$ core levels; SEM images of the thin films; lateral electrical conductivity measurements and photoelectrochemical characterization of the bare FTO substrate (PDF)

AUTHOR INFORMATION

Corresponding Author

Nicolas D. Boscher − *Luxembourg Institute of Science and Technology, Materials Research and Technology Department, L-4422 Belvaux, Luxembourg;* orcid.org/0000-0003-3693-6866; Phone: +352275888578; Email: Nicolas.boscher@list.lu

Authors

Ali M. Huerta-Flores − *Luxembourg Institute of Science and Technology, Materials Research and Technology Department, L-4422 Belvaux, Luxembourg; Universidad Autonoma de Nuevo Leon, Facultad de Ingenieria Civil, Departmento de Ecomateriales y Energia, Av. Universidad S/N Ciudad Universitaria, Nuevo Leon, C.P. 66455, Mexico*

Giuseppe Bengasi − *Luxembourg Institute of Science and Technology, Materials Research and Technology Department, L-4422 Belvaux, Luxembourg*

Kamal Baba − *Luxembourg Institute of Science and Technology, Materials Research and Technology Department, L-4422 Belvaux, Luxembourg;* orcid.org/0000-0002-8405-035X

Complete contact information is available at: https://pubs.acs.org/10.1021/acsaem.0c01545

Author Contributions

The manuscript was written through contributions of all authors. All authors have given approval to the final version of the manuscript.

Funding

This project has received funding from the European Research Council (ERC) under the European Union's Horizon 2020 research and innovation program (grant agreement no. 865985) and from the Luxembourg National Research Fund (FNR) through the project PLASPEROX (Industrial Fellowships/19/13711983).

Notes

The authors declare no competing financial interest.

ACKNOWLEDGMENTS

We gratefully acknowledge the financial support of the European Research Council (ERC) through the ERC Consolidator Grant project CLEANH2 (grant agreement no. 865985). A.M.H.-F. is particularly grateful to the Luxembourg National Research Fund (FNR) for supporting her postdoctoral position at LIST through the PLASPEROX project (Industrial Fellowships/19/13711983). D. El Assad, Dr. G. Frache, Dr. J. Guillot, C. Vergne, and J.-L. Biagi from LIST are acknowledged for the HRMS, XPS, and SEM measurements.

REFERENCES

(1) Zhang, W.; Lai, W.; Cao, R. Energy-Related Small Molecule Activation Reactions: Oxygen Reduction and Hydrogen and Oxygen Evolution Reactions Catalyzed by Porphyrin- and Corrole-Based Systems. *Chem. Rev.* **2017**, *117*, 3717−3797.

(2) Khusnutdinova, D.; Wadsworth, B. L.; Flores, M.; Beiler, A. M.; Reyes Cruz, E. A.; Zenkov, Y.; Moore, G. F. Electrocatalytic Properties of Binuclear Cu(II) Fused Porphyrins for Hydrogen Evolution. *ACS Catal.* **2018**, *8*, 9888−9898.

(3) Ladomenou, K.; Natali, M.; Iengo, E.; Charalampidis, G.; Scandola, F.; Coutsolelos, A. G. Photochemical Hydrogen Generation with Porphyrin-Based Systems. *Coord. Chem. Rev.* **2015**, *304*−*305*, 38−54.

(4) Jia, H.; Sun, Z.; Jiang, D.; Du, P. Covalent Cobalt Porphyrin Framework on Multiwalled Carbon Nanotubes for Efficient Water Oxidation at Low Overpotential. *Chem. Mater.* **2015**, *27*, 4586−4593.

(5) Hijazi, I.; Bourgeteau, T.; Cornut, R.; Morozan, A.; Filoramo, A.; Leroy, J.; Derycke, V.; Jousselme, B.; Campidelli, S. Carbon Nanotube-Templated Synthesis of Covalent Porphyrin Network for Oxygen Reduction Reaction. *J. Am. Chem. Soc.* **2014**, *136*, 6348−6354.

(6) Wan, H.; Jensen, A.; Escudero-Escribano, M.; Rossmeisl, J. Insights in the Oxygen Reduction Reaction: from Metallic Electrocatalysts to Diporphyrines. *ACS Catal.* **2020**, *10*, 5979−5989.

(7) Shan, B.; Nayak, A.; N. Sampaio, R.; Eberhart, M. S.; Troian-Gautier, L.; Brennaman, M. K.; Meyer, G. J.; Meyer, T. J. Direct Photoactivation of a Nickel-Based, Water-Reduction Photocathode by

a Highly Conjugated Supramolecular Chromophore. *Energy Environ. Sci.* **2018**, *11*, 447−455.
(8) Aziz, A.; Ruiz-Salvador, A. R.; Hernandez, N. C.; Calero, S.; Hamad, S.; Grau-Crespo, R. Porphyrin-Based Metal-Organic Frameworks for Solar Fuel Synthesis Photocatalysis: Band Gap Tuning via Iron Substitutions. *J. Mater. Chem. A* **2017**, *5*, 11894−11904.
(9) Xie, L.; Tian, J.; Ouyang, Y.; Guo, X.; Zhang, W.; Apfel, U. P.; Zhang, W.; Cao, R. Water-Soluble Polymers with Appending Porphyrins as Bioinspired Catalysts for the Hydrogen Evolution Reaction. *Angew. Chem., Int. Ed.* **2020**, DOI: 10.1002/anie.202003836.
(10) Wang, N.; Lei, H.; Zhang, Z.; Li, J.; Zhang, W.; Cao, R. Electrocatalytic Hydrogen Evolution with Gallium Hydride and Ligand-Centered Reduction. *Chem. Sci.* **2019**, *10*, 2308−2314.
(11) Guo, X.; Wang, N.; Li, X.; Zhang, Z.; Zhao, J.; Ren, W.; Ding, S.; Xu, G.; Li, J.; Apfel, U.-P.; Zhang, W.; Cao, R. Homolytic versus Heterolytic Hydrogen Evolution Reaction Steered via Steric Effect. *Angew. Chem., Int. Ed.* **2020**, *59*, 8941−8946.
(12) Wang, Y.; Silveri, F.; Bayazit, M. K.; Ruan, Q.; Li, Y.; Xie, J.; Catlow, C. R. A.; Tang, J. Bandgap Engineering of Organic Semiconductors for Highly Efficient Photocatalytic Water Splitting. *Adv. Energy Mater.* **2018**, *8*, 1801084.
(13) Woods, D. J.; Sprick, R. S.; Smith, C. L.; Cowan, A. J.; Cooper, A. I. A Solution-Processable Polymer Photocatalyst for Hydrogen Evolution from Water. *Adv. Energy Mater.* **2017**, *7*, 1700479.
(14) Cao, S.; Low, J.; Yu, J.; Jaroniec, M. Polymeric Photocatalysts Based on Graphitic Carbon Nitride. *Adv. Mater.* **2015**, *27*, 2150−2176.
(15) Chen, W.; Akhigbe, J.; Brückner, C.; Li, C. M.; Lei, Y. Electrocatalytic Four-Electron Reduction of Dioxygen by Electrochemically Deposited Poly{[meso-Tetrakis(2-Thienyl)Porphyrinato]-Cobalt(II)}. *J. Phys. Chem. C* **2010**, *114*, 8633−8638.
(16) Tanaka, T.; Osuka, A. Conjugated Porphyrin Arrays: Synthesis, Properties and Applications for Functional Materials. *Chem. Soc. Rev.* **2015**, *44*, 943−969.
(17) Tsuda, A.; Osuka, A. Fully Conjugated Porphyrin Tapes with Electronic Absorption Bands that Reach into Infrared. *Science* **2001**, *293*, 79−82.
(18) Auwärter, W.; Écija, D.; Klappenberger, F.; Barth, J. V. Porphyrins at Interfaces. *Nat. Chem.* **2015**, *7*, 105−120.
(19) He, Y.; Garnica, M.; Bischoff, F.; Ducke, J.; Bocquet, M.-L.; Batzill, M.; Auwärter, W.; Barth, J. V. Fusing Tetrapyrroles to Graphene Edges by Surface-Assisted Covalent Coupling. *Nat. Chem.* **2017**, *9*, 33−38.
(20) Bengasi, G.; Baba, K.; Frache, G.; Desport, J.; Gratia, P.; Heinze, K.; Boscher, N. D. Conductive Fused Porphyrin Tapes on Sensitive Substrates by a Chemical Vapor Deposition Approach. *Angew. Chem., Int. Ed.* **2019**, *58*, 2103−2108.
(21) Bengasi, G.; Quétu, L.; Baba, K.; Ost, A.; Cosas Fernandes, J. P.; Grysan, P.; Heinze, K.; Boscher, N. D. Constitution and Conductivity of Metalloporphyrin Tapes. *Eur. J. Inorg. Chem.* **2020**, *2020*, 1938−1945.
(22) Bengasi, G.; Desport, J. S.; Baba, K.; Cosas Fernandes, J. P.; De Castro, O.; Heinze, K.; Boscher, N. D. Molecular Flattening Effect to Enhance the Conductivity of Fused Porphyrin Tapes Thin Films. *RSC Adv.* **2020**, *10*, 7048−7057.
(23) Heydari Gharahcheshmeh, M.; Gleason, K. K. Device Fabrication Based on Oxidative Chemical Vapor Deposition (oCVD) Synthesis of Conducting Polymers and Related Conjugated Organic Materials. *Adv. Mater. Interfaces* **2019**, *6*, 1801564.
(24) Bengasi, G.; Baba, K.; Back, O.; Frache, G.; Heinze, K.; Boscher, N. D. Reactivity of Nickel(II) Porphyrins in oCVD Processes—Polymerisation, Intramolecular Cyclisation and Chlorination. *Chem. - Eur. J.* **2019**, *25*, 8313−8320.
(25) Baba, K.; Bengasi, G.; El Assad, D.; Grysan, P.; Lentzen, E.; Heinze, K.; Frache, G.; Boscher, N. D. Conductive Directly Fused Poly(Porphyrin) Coatings by Oxidative Chemical Vapour Deposition − From Single- to Triple-Fused. *Eur. J. Org. Chem.* **2019**, *2019*, 2368−2375.
(26) Rubires, R.; Crusats, J.; El-Hachemi, Z.; Jaramillo, T.; Lopez, M.; Valls, E.; Farrera, J.-A.; Ribo, J. M. Self-Assembly in Water of the Sodium Salts of Meso-Sulfonatophenyl Substituted Porphyrins. *New J. Chem.* **1999**, *23*, 189−198.
(27) Presselt, M.; Dehaen, W.; Maes, W.; Klamt, A.; Martínez, T.; Beenken, W. J. D.; Kruk, M. Quantum Chemical Insights into the Dependence of Porphyrin Basicity on the *meso*-aryl Substituents: Thermodynamics, Buckling, Reaction Sites and Molecular Flexibility. *Phys. Chem. Chem. Phys.* **2015**, *17*, 14096−14106.
(28) Hooley, J. G.; Sams, J. R.; Liengme, B. V. The Effect of Flake Size on the Mössbauer Spectrum of Graphite Ferrous Chloride. *Carbon* **1970**, *8*, 467−471.
(29) Wijesekera, T.; Matsumoto, A.; Dolphin, D.; Lexa, D. Perchlorinated and Highly Chlorinated meso-Tetraphenylporphyrins. *Angew. Chem., Int. Ed. Engl.* **1990**, *29*, 1028−1030.
(30) Reid, I.; Zhang, Y.; Demasi, A.; Blueser, A.; Piper, L.; Downes, J. E.; Matsuura, A.; Hughes, A.; Smith, K. E. Electronic Structure of the Organic Semiconductor Copper Tetraphenylporphyrin (CuTPP). *Appl. Surf. Sci.* **2009**, *256*, 720−725.
(31) Sakurai, T.; Tashiro, K.; Honsho, Y.; Saeki, A.; Seki, S.; Osuka, A.; Muranaka, A.; Uchiyama, M.; Kim, J.; Ha, S.; Kato, K.; Takata, M.; Aida, T. Electron- or Hole-Transporting Nature Selected by Side-Chain-Directed π-Stacking Geometry: Liquid Crystalline Fused Metalloporphyrin Dimers. *J. Am. Chem. Soc.* **2011**, *133*, 6537−6540.
(32) Cesar, I.; Sivula, K.; Kay, A.; Zboril, R.; Grätzel, M. Influence of Feature Size, Film Thickness, and Silicon Doping on the Performance of Nanostructured Hematite Photoanodes for Solar Water Splitting. *J. Phys. Chem. C* **2009**, *113*, 772−782.
(33) McCrory, C. C. L.; Jung, S.; Ferrer, I. M.; Chatman, S. M.; Peters, J. C.; Jaramillo, T. F. Benchmarking Hydrogen Evolving Reaction and Oxygen Evolving Reaction Electrocatalysts for Solar Water Splitting Devices. *J. Am. Chem. Soc.* **2015**, *137*, 4347−4357.
(34) Zeng, M.; Li, Y. Recent Advances in Heterogeneous Electrocatalysts for Hydrogen Evolution Reaction. *J. Mater. Chem. A* **2015**, *3*, 14942−14962.
(35) Vesborg, P. C. K.; Seger, B.; Chorkendorff, I. Recent Development in Hydrogen Evolution Reaction Catalysts and Their Practical Implementation. *J. Phys. Chem. Lett.* **2015**, *6*, 951−957.
(36) Kong, D. S.; Wang, H. T.; Cha, J. J.; Pasta, M.; Koski, K. J.; Yao, J.; Cui, Y. Synthesis of MoS_2 and $MoSe_2$ Films with Vertically Aligned Layers. *Nano Lett.* **2013**, *13*, 1341−1347.
(37) Bellamkonda, S.; Shanmugam, R.; Gangavarapu, R. R. Extending the π-electron Conjugation in 2D Planar Graphitic Carbon Nitride: Efficient Charge Separation for Overall Water Splitting. *J. Mater. Chem. A* **2019**, *7*, 3757−3771.
(38) Fateeva, A.; Chater, P. A.; Ireland, C. P.; Tahir, A. A.; Khimyak, Y. Z.; Wiper, P. V.; Darwent, J. R.; Rosseinsky, M. J. A Water-Stable Porphyrin-Based Metal−Organic Framework Active for Visible-Light Photocatalysis. *Angew. Chem., Int. Ed.* **2012**, *51*, 7440.
(39) Meng, J.; Bi, P.; Jia, J.; Sun, X.; Chen, R. Light-Assisted Catalytic Water Oxidation from Porphyrin J-Aggregate. *ChemistrySelect* **2017**, *2*, 4882−4888.
(40) Chen, Y.; Li, A.; Huang, Z. H.; Wang, L. N.; Kang, F. Porphyrin-Based Nanostructures for Photocatalytic Applications. *Nanomaterials* **2016**, *6*, 51.
(41) Chen, Y.; Huang, Z. H.; Yue, M.; Kang, F. Integrating Porphyrin Nanoparticles into a 2D Graphene Matrix for Free-Standing Nanohybrid Films with Enhanced Visible-Light Photocatalytic Activity. *Nanoscale* **2014**, *6*, 978−985.
(42) Vinodh, M.; Alipour, F. H.; Mohamod, A. A.; Al-Azemi, T. F. Molecular Assemblies of Porphyrins and Macrocyclic Receptors: Recent Developments in Their Synthesis and Applications. *Molecules* **2012**, *17*, 11763−11799.

https://dx.doi.org/10.1021/acsaem.0c01545
ACS Appl. Energy Mater. 2020, 3, 9848−9855